Front. Mech. Eng.
DOI 10.1007/s11465-017-0420-7

RESEARCH ARTICLE

Shuaishuai WANG, Caichao ZHU, Chaosheng SONG, Huali HAN

Effects of elastic support on the dynamic behaviors of the wind turbine drive train

Abstract The reliability and service life of wind turbines are influenced by the complex loading applied on the hub, especially amidst a poor external wind environment. A three-point elastic support, which includes the main bearing and two torque arms, was considered in this study. Based on the flexibilities of the planet carrier and the housing, a coupled dynamic model was developed for a wind turbine drive train. Then, the dynamic behaviors of the drive train for different elastic support parameters were computed and analyzed. Frequency response functions were used to examine how different elastic support parameters influence the dynamic behaviors of the drive train. Results showed that the elastic support parameters considerably influenced the dynamic behaviors of the wind turbine drive train. A large support stiffness of the torque arms decreased the dynamic response of the planet carrier and the main bearing, whereas a large support stiffness of the main bearing decreased the dynamic response of planet carrier while increasing that of the main bearing. The findings of this study provide the foundation for optimizing the elastic support stiffness of the wind turbine drive train.

Keywords wind turbine drive train, elastic support, dynamic behavior, frequency response function

1 Introduction

The wind turbine drive train is a key component of wind turbines, and the performance of the former is responsible for the reliability and service life of the latter. An elastic support condition for the drive train can directly affect the inherent characteristics and dynamic response of the coupled wind turbine drive train system. Therefore, the effects of the elastic support on the dynamics of the wind turbine drive train must be elucidated to improve the reliability and service life of wind turbines.

Recent studies on the dynamic performance and operation stability of the wind turbine drive train have been conducted. For example, Guo et al. [1,2] developed a dynamic model of the wind turbine gearbox based on the three-point elastic support; they also analyzed the combined effects of gravity, bending moment, bearing clearance, and input torque on the load sharing of the wind turbine planetary gear. Helsen et al. [3,4] utilized a flexible multibody modeling technique to establish a dynamic model of the wind turbine gearbox; they then discussed the effects of different elastic support modes on its dynamic characteristics. Jin et al. [5] compared and analyzed the dynamic behaviors of the three modes (i.e., multi-rigid body model of pure torsion, multi-rigid body model with six degrees of freedom (DOFs), and multi-flexible body model), and found that the multi-flexible body model can most accurately reflect the dynamic performance of the wind turbine gearbox. He et al. [6] established a multi-flexible body dynamics simulation model of the wind turbine drive train, and identified the risk resonance points by applying the integrated time domain and frequency domain methods. Meanwhile, Ericson and Parker [7] conducted experiments to examine the effects of torque on the inherent characteristics and dynamic response of planetary gears. Zhao and Ji [8] developed a wind turbine transmission model with two-stage planetary transmission and one-stage parallel shaft transmission, and then compared the effects of external excitation and several internal excitations on the torsional vibration of the system. Wei et al. [9] evaluated how various uncertain system parameters affected the dynamic response of the wind turbine gearbox. In another study, Yi et al. [10] established a wind turbine gearbox coupled dynamic model, which

Received September 9, 2016; accepted November 23, 2016

Shuaishuai WANG, Caichao ZHU (✉), Chaosheng SONG
The State Key Laboratory of Mechanical Transmissions, Chongqing University, Chongqing 400030, China
E-mail: cczhu@cqu.edu.cn

Huali HAN
CSIC (Chongqing) Haizhuang Windpower Equipment Co., Ltd., Chongqing 401122, China

considers several nonlinear factors, such as the time-varying meshing stiffness, the time-varying external load, and the dynamic transmission error; they also studied the load-sharing characteristics of the system. Zhu et al. [11,12] proposed a dynamic model of a wind turbine gearbox with flexible pins, and then analyzed the dynamic behaviors of the wind turbine drive train with respect to the load spectrum. Finally, Zhai et al. [13] used the lumped parameter method to establish a bending-torsion-pendulum coupled dynamic model for a planetary gear system; they then analyzed the influences of planet carrier installation errors on the dynamic characteristics.

In the current study, a 2 MW wind turbine drive train was selected as the research object, in order to investigate the effects of different elastic support parameters on the dynamic characteristics.

2 Transmission principles and dynamic modeling of the wind turbine drive train

2.1 Transmission principles

The 2 MW wind turbine drive train used in this study mainly consisted of a hub, a main shaft, a gearbox, a flexible coupling, and a generator. Figure 1 shows the transmission principle diagram of the wind turbine drive train. Wind energy was first converted by the blade into the twisting mechanical energy acting on the hub. Then, the rotation energy was transmitted through the main shaft to the gearbox, which transformed the low-speed, high-torque mechanical energy into a high-speed, low-torque form. Finally, the generator was driven by flexible coupling to generate electricity. The gearbox, which consisted of a planet stage and two parallel stages with an overall transmission ratio of 1:115.24, is an important component of the wind turbine drive train. For the first planetary gear transmission stage, the ring gear was fixed, the planet carrier served as the torque input, and the sun gear was the torque output. For the second and third parallel shaft transmission stages, the power from the sun gear first transited to the middle stage gear pair (G_1-G_2) and then delivered to the high-speed shaft through the high-speed gear pair (G_3-G_4). The detailed structural and material parameters of the drive train are listed in Tables 1–3.

2.2 Dynamic modeling

For the modeling, the bedplate and the nacelle were considered as one component. The wind turbine drive train was supported in three locations, namely, the main bearing and two torque arms. Figure 2 shows the topology diagram. This was established based on the installation relationship and transmission principle of the wind turbine drive train. The basic elements of the topology diagram consisted of the body, the joint, and the force element. The body represented the components of the drive train, the joint referred to motion constrains, and the force element denoted the interaction among the components of the drive train. The topological graph illustrates the relationship among the components of the wind turbine drive train. The symbols appearing in Fig. 2 are described in Table 4.

As shown in Fig. 2, the hub is connected to the main shaft, which is linked to the planet carrier by the locking disk. Three planets are installed on the carrier, and all of them engage with both the sun gear and ring gear. One end of the coupling element is connected to the high-speed shaft, and the other is connected to the generator. The planet carrier, the splined shaft, the middle-speed shaft, and the high-speed shaft are supported on the housing by bearings. The main shaft, the gearbox housing, and the generator are supported on the nacelle by the main bearing, the torque arms, and the generator holder, respectively. The nacelle is attached to the ground with fixed constraints.

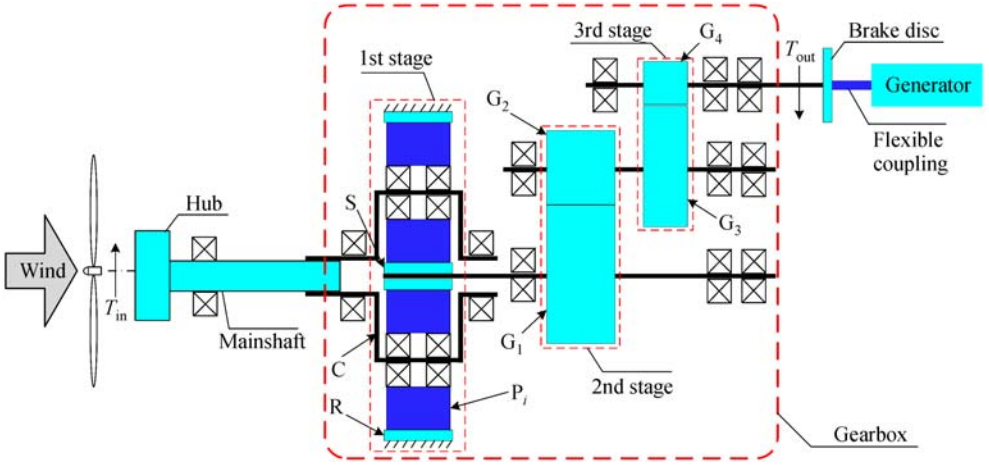

Fig. 1 Diagram of the transmission principle of the wind turbine drive train

R–The internal ring; C–The carrier; P_i–The planet gears; S–The sun gear; G_1 and G_2–The wheel and gear of the middle gear stage, respectively; G_3 and G_4–The wheel and gear of the high-speed gear stage, respectively; T_{in}–The input torque; T_{out}–The output torque

Table 1 Main structural parameters of the wind turbine drive train

Parameter	Value	Parameter	Value
Rated power	2200 kW	Cut-in wind speed	3 m/s
Transmission ratio	1:115.24	Rated wind speed	10 m/s
Design life	20 years	Cut-out wind speed	25 m/s
Number of blades	3	Main shaft length	2.9 m
Blade length	39 m	Hub height	80.6 m
Direction of rotation	Clockwise	Rated speed	1790 r/min
Quality of blades	38 t	Types of the generator	Asynchronous doubly-fed

Table 2 Gearbox parameters

Stage	Gear	Number of teeth	Module/mm	Pressure angle/(°)	Helix angle/(°)	Transmission ratio
1st	Sun gear	21	15	8	25	5.571
	Planet gear	37	15	8	25	5.571
	Ring gear	96	15	8	25	5.571
2nd	Wheel	97	11	10	20	4.217
	Pinion	23	11	10	20	4.217
3rd	Wheel	103	8	10	20	4.905
	Pinion	21	8	10	20	4.905

Table 3 Material parameters of the wind turbine drive train

Component	Material	Density/(kg·m^{-3})	Young's modulus/GPa	Poisson's ratio
Hub and housing	QT400	7.01×10^3	161	0.274
Carrier	QT700	7.09×10^3	169	0.305
Gears and shafts	Steel	7.85×10^3	216	0.310

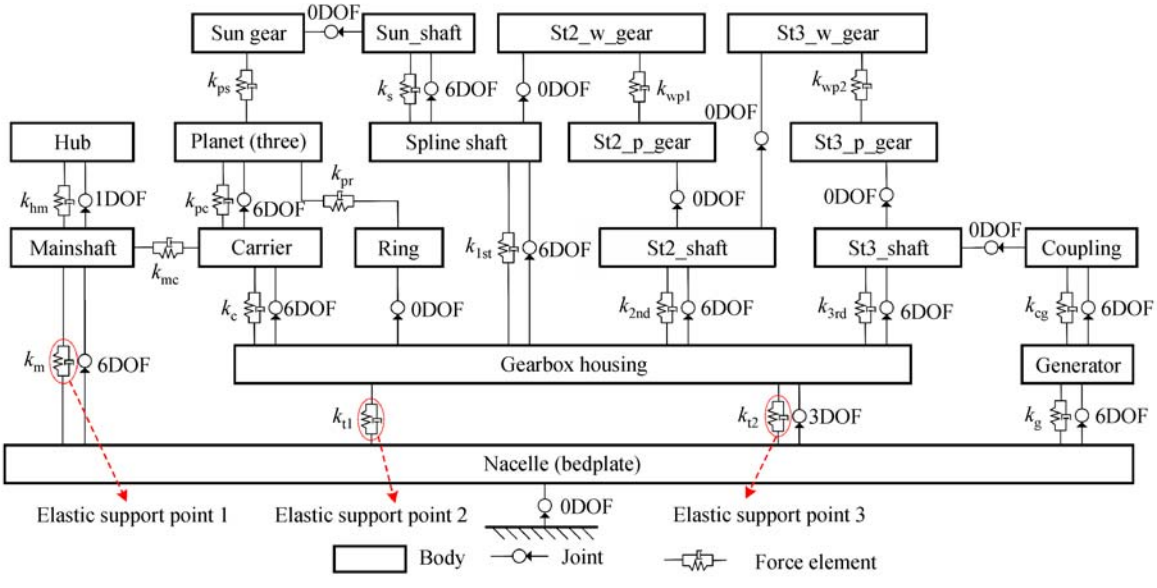

Fig. 2 Topology graph of the wind turbine drive train model

St2_w/p_gear–The wheel and gear of the middle gear stage, respectively; St3_w/p_gear–The wheel and gear of the high-speed gear stage, respectively; St2/St3_shaft–The middle speed shaft and the high-speed shaft, respectively

Table 4 Symbols in the topological graph of the drive train

Symbol	Representation	Symbol	Representation
k_{hm}	Torsional stiffness and damping of the hub	k_{cg}	Torsional stiffness and damping of the coupling
k_{mc}	Stiffness and damping of the locking disk	k_{c}	Bearing stiffness and damping of the planet carrier
k_{pc}	Bearing stiffness and damping of planets	k_{1st}	Bearing stiffness and damping of the spline shaft
k_{ps}	Meshing stiffness and damping sun-planet gear pair	k_{2nd}	Bearing stiffness and damping of the middle stage shaft
k_{pr}	Meshing stiffness and damping ring-planet gear pair	k_{3rd}	Bearing stiffness and damping of high-the speed stage shaft
k_{s}	Spline stiffness and damping	k_{m}	Bearing stiffness and damping of the main shaft
k_{wp1}	Meshing stiffness and damping middle stage gear pair	k_{t1}/k_{t2}	Elastic supporting stiffness and damping of the torque arms
k_{wp2}	Meshing stiffness and damping high-speed stage gear pair	k_{g}	Elastic supporting stiffness and damping of the generator

The elastic support of the torque arms and all bearings of the drive train were simulated using spring elements with six DOFs in six directions. The relationship of the external loads ($F_{\text{body},i}$ ($i=1, 2$)) acting on the bearings and the relative displacements ($q_{\text{body},i}$ ($i=1, 2$)) between the two ends of the bearing can be expressed as [6]

$$\begin{bmatrix} \boldsymbol{F}_{\text{body},1} \\ \boldsymbol{F}_{\text{body},2} \end{bmatrix} = \boldsymbol{K}_{\text{bearing}} \begin{bmatrix} \boldsymbol{q}_{\text{body},1} \\ \boldsymbol{q}_{\text{body},2} \end{bmatrix} + \boldsymbol{C}_{\text{bearing}} \begin{bmatrix} \dot{\boldsymbol{q}}_{\text{body},1} \\ \dot{\boldsymbol{q}}_{\text{body},2} \end{bmatrix}, \quad (1)$$

where

$$\boldsymbol{F}_{\text{body},1} = [F_{X1}\ F_{Y1}\ F_{Z1}\ M_{X1}\ M_{Y1}\ M_{Z1}]^{\text{T}}, \quad (2)$$

$$\boldsymbol{F}_{\text{body},2} = [F_{X2}\ F_{Y2}\ F_{Z2}\ M_{X2}\ M_{Y2}\ M_{Z2}]^{\text{T}}, \quad (3)$$

$$\boldsymbol{q}_{\text{body},1} = [x_1\ y_1\ z_1\ \theta_{x1}\ \theta_{y1}\ \theta_{z1}]^{\text{T}}, \quad (4)$$

$$\boldsymbol{q}_{\text{body},2} = [x_2\ y_2\ z_2\ \theta_{x2}\ \theta_{y2}\ \theta_{z2}]^{\text{T}}, \quad (5)$$

$$\boldsymbol{K}_{\text{bearing}} = \begin{bmatrix} K_{xx} & 0 & 0 & 0 & 0 & 0 \\ 0 & K_{yy} & 0 & 0 & 0 & 0 \\ 0 & 0 & K_{zz} & 0 & 0 & 0 \\ 0 & 0 & 0 & 0 & 0 & 0 \\ 0 & 0 & 0 & 0 & K_{uu} & 0 \\ 0 & 0 & 0 & 0 & 0 & K_{vv} \end{bmatrix}. \quad (6)$$

In Eqs. (1)–(6), $\boldsymbol{K}_{\text{bearing}}$ is the stiffness matrix of the bearings, $\boldsymbol{C}_{\text{bearing}}$ is the damping matrix of the bearings, and K_{aa} ($a=x, y, z, u, v$) is the elements of the stiffness matrix with different DOF.

Frequency response functions (FRFs) were used to investigate the effects of different elastic support parameters on the dynamic behaviors of the drive train. FRFs were applied to describe the physical quantities of a system's gain and phase with frequency variation to reflect the characteristics of the system. Linear analysis of the system was conducted to realize the FRF-based approach. To calculate the mesh stiffness, each gear was divided into strips across the contact line. The stiffness between each pair of strips of the pinion and the gear was then calculated in accordance with ISO 6336. Consequently, the synthesized mesh stiffness for the gear pair can be obtained [14]. Except for the planet carrier and the housing, all structural components were considered rigid. Then, the finite element models for the planet carrier and the housing were condensed to reduced stiffness matrices, which were connected to the transmission components by interface nodes. The rigid-flexible coupled multi-body dynamic model (Fig. 3) was developed using the commercial software SIMPACK [15]. In the model, the hub has one rotational DOF with respect to the main shaft. Meanwhile, the main shaft, the planets, the sun shaft, the spline shaft, the middle-speed shaft, the high-speed shaft, the coupling, and the generator have six DOFs in each direction. Thus, the entire drive train dynamic model has 61 DOFs.

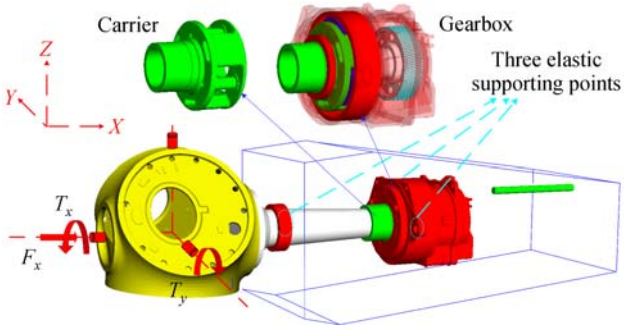

Fig. 3 Dynamic model of the wind turbine drive train

3 Dynamic analysis of the wind turbine drive train

The main excitations on the hub center, namely, torque loading (T_x), pitch loading (T_y), and thrust loading (F_x), considerably influence the dynamic performance of the drive train [16–18]. Excitations along two rotational coordinates (r_x, r_y) and one translational coordinate (x) were applied on the hub center, as shown in Fig. 3. The bearing coordinate point on the planet carrier in the

downwind direction and the main bearing coordinate point on the main shaft were selected as the critical points for measuring the dynamic response. A spring element with damping was used to simulate the main bearing, and the dynamic performance of the main bearing coordinate point can accurately reveal the dynamic behaviors of the main bearing. Three translational coordinate (x, y, z) directions and two rotational coordinate (r_y, r_z) directions were considered to determine the response from the critical points.

The FRFs between the different excitation directions and response directions were calculated. The FRF between the excitation in the hub center and the response on the defined point in the carrier is the displacement frequency response, which reflects the motion performance of the planet carrier with respect to the gearbox. Another FRF corresponding to the main bearing is the force frequency response, which reflects the force performance of the main bearing. The effects of the elastic support parameters on the dynamic behaviors of the drive train can be determined by comparing the change in each FRF for the different elastic supporting parameters. Given that the main load excitation frequency at the hub had low frequency during the normal operation of the drive train, the excitation frequency and the analysis frequency were mainly defined to be in the low-frequency range between 0 and 25 Hz [3,19].

3.1 Effects of the elastic support stiffness of the torque arms

The effects of elastic support stiffness of the torque arms on the dynamic behaviors of the drive train are discussed in this section. The elastic support stiffness in the vertical direction (z) plays an essential role in the dynamic performance of wind turbine drive train [20]. The normal elastic support stiffness in the vertical direction (z) was defined as X. The dynamic behaviors of the drive train for three kinds of elastic support stiffness of the torque arms were compared and analyzed. Figure 4 shows the FRFs

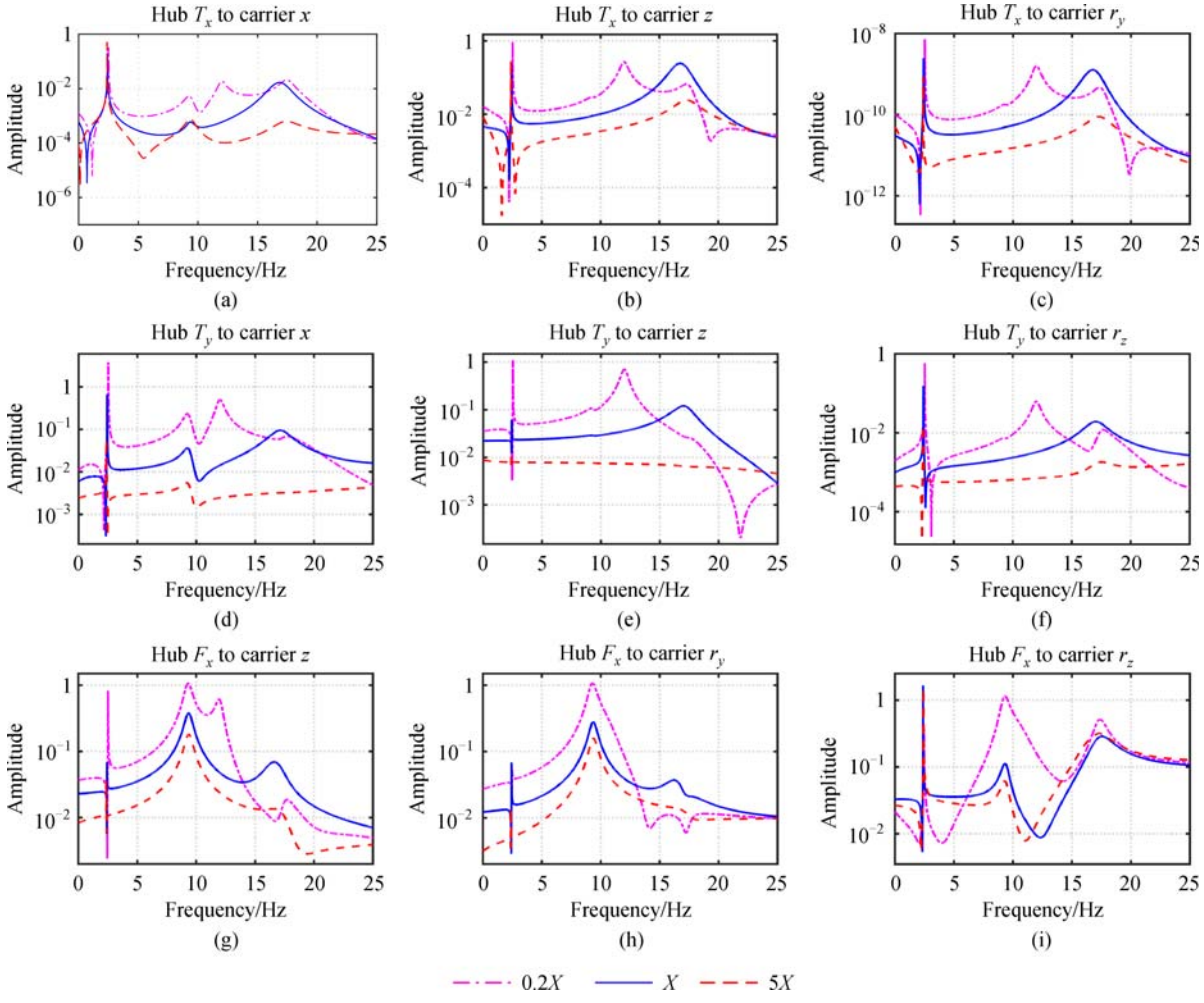

Fig. 4 FRFs between the hub center excitation and the planet carrier response for different elastic supporting stiffness of the torque arms. (a) Hub T_x to carrier x; (b) hub T_x to carrier z; (c) hub T_x to carrier r_y; (d) hub T_y to carrier x; (e) hub T_y to carrier z; (f) hub T_y to carrier r_z; (g) hub F_x to carrier z; (h) hub F_x to carrier r_y; (i) hub F_x to carrier r_z

Hub T_x to carrier x–The FRF between the hub center excitation in the T_x direction and the response in the x direction of the bearing coordinate point on the planet carrier in the downwind direction

between hub center excitation and planet carrier response for different elastic support stiffness of the torque arms.

The results indicate that variations in the radial (z) support stiffness of the torque arms considerably influence the dynamic performance of the planet carrier. The increase in the radial (z) support stiffness of the torque arms decreases the dynamic response of the planet carrier in each coordinate direction, suggesting that the dynamic performances of the planet carrier will be improved. Figure 5 shows the FRFs between the hub center excitation and the main bearing response for different elastic supporting stiffness of the torque arms.

Variations in the radial (z) support stiffness of the torque arm considerably influence the dynamic performance of the main bearing. An increase in the radial (z) support stiffness of the torque arm decreases the dynamic response of the main bearing.

A comprehensive analysis of Figs. 4 and 5 reveals that a better dynamic performance of the drive train can be obtained with a higher radial (z) support stiffness of the torque arms. The main purpose of the elastic support design of the torque arms is to reduce the vibration transferred from the gearbox to the nacelle and the tower as well as the noise generated by the gear meshing. Therefore, the elastic support damping of the torque arms plays an important role, and can be expressed as [21]

$$d = 2D\sqrt{KM}, \tag{7}$$

where D is the damping coefficient of elastic support, K is the linear stiffness of elastic support, and M is the equivalent mass.

According to Eq. (7), a larger stiffness of the elastic support system corresponds to a larger damping value. However, if the damping value is extremely high, the reduction of vibration and noise becomes weaker.

The comprehensive analysis also indicates that the large and a small elastic support stiffness of the torque arms manifest adverse dynamic characteristics of the drive train.

3.2 Effects of main bearing stiffness

The effects of the variations in the main bearing stiffness on the dynamic performance of the drive train are discussed in this section. The normal value of the main bearing stiffness was defined as X. The dynamic behaviors of the drive train for three kinds of main bearing stiffness were computed and compared. Figure 6 shows the FRFs between the hub center excitation and the planet carrier response for different main bearing stiffness.

Variations in the main bearing stiffness exerts a weak influence on the dynamic response of the planet carrier. Nonetheless, a higher main bearing stiffness generally corresponds to a decrease in the dynamic response of the planet carrier in each coordinate direction. In addition, variations in the main shaft bearing stiffness changed the

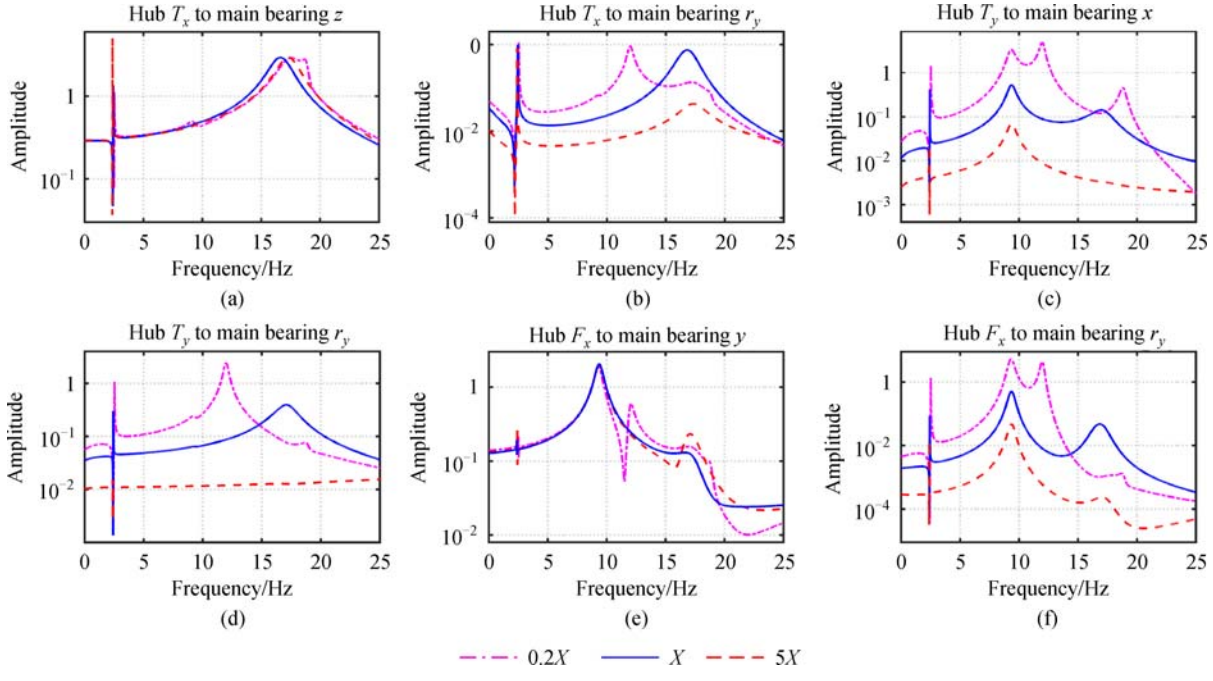

Fig. 5 FRFs between the hub center excitation and the main bearing response for different elastic supporting stiffness of the torque arms. (a) Hub T_x to main bearing z; (b) hub T_x to main bearing r_y; (c) hub T_y to main bearing x; (d) hub T_y to main bearing r_y; (e) hub F_x to main bearing y; (f) hub F_x to main bearing r_y

Hub T_x to main bearing z–The FRF between the hub center excitation in the T_x direction and the response in the z direction of the bearing coordinate point on the main shaft

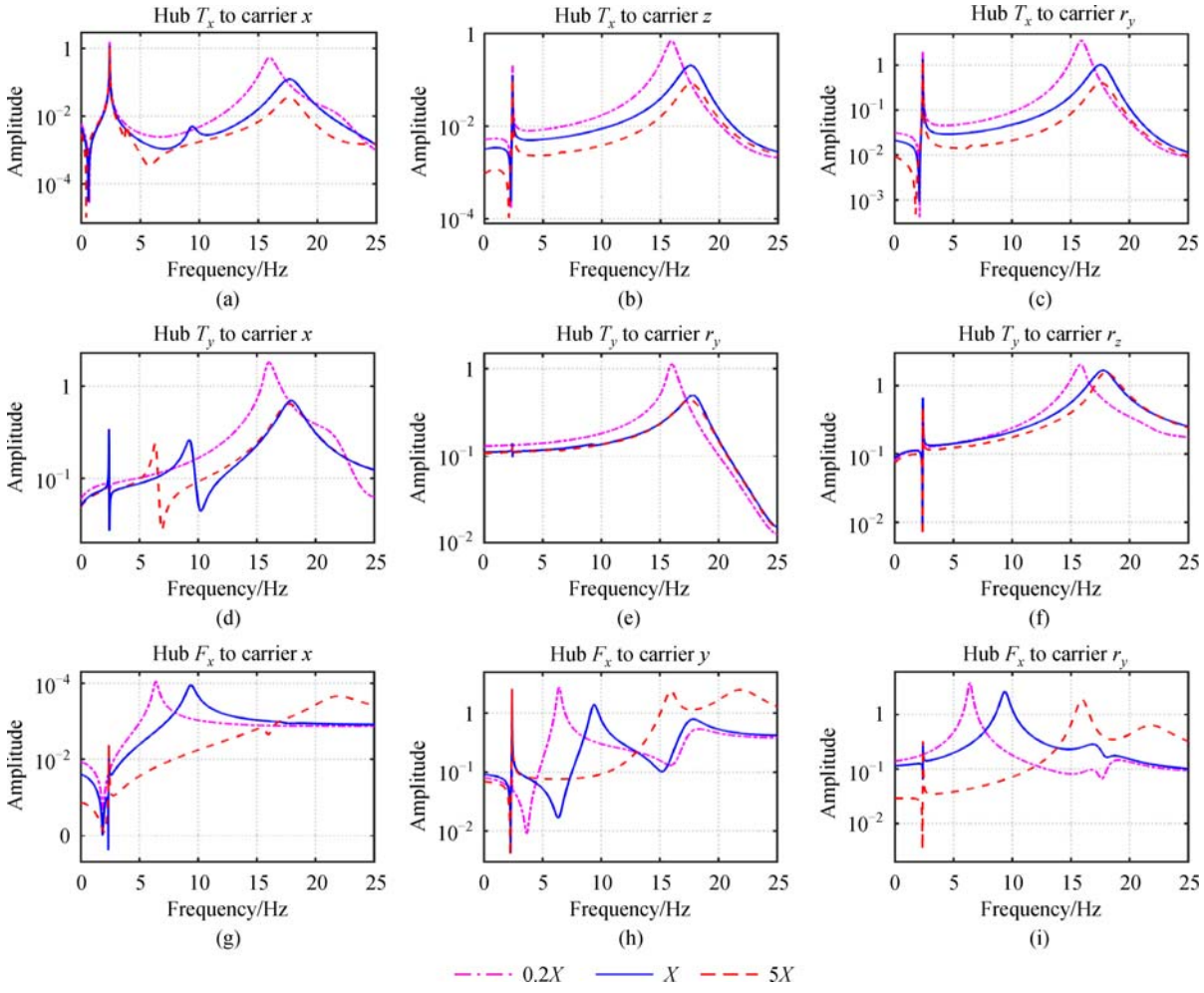

Fig. 6 FRFs between the hub center excitation and the planet carrier response for different main bearing stiffness. (a) Hub T_x to carrier x; (b) hub T_x to carrier z; (c) hub T_x to carrier r_y; (d) hub T_y to carrier x; (e) hub T_y to carrier r_y; (f) hub T_y to carrier r_z; (g) hub F_x to carrier x; (h) hub F_x to carrier y; (i) hub F_x to carrier r_y

Hub T_x to carrier x–The FRF between the hub center excitation in the T_x direction and the response in the x direction of the bearing coordinate point on the planet carrier in the downwind direction

locations of the response peaks of the planet carrier. The frequency of the peak response is 9.4 Hz for the normal main shaft bearing stiffness; this value is reduced to 6.4 Hz for 0.2 times of the normal stiffness and then increased to 15.9 Hz for five times of the normal stiffness. Figure 7 shows the FRFs between the hub center excitation and the main bearing response for different main bearing stiffness.

The results indicate that variations in the main bearing stiffness considerably influence the dynamic performance of the main bearing. A higher main bearing stiffness increases the dynamic response of the main bearing. In addition, variations in the main shaft bearing stiffness change the locations of the response peaks of the main bearing. The frequency of the peak response is 9.4 Hz for the normal main shaft bearing stiffness; this value is reduced to 3.8 Hz for 0.2 times of the normal stiffness and then increased to 15.9 Hz for five times of the normal stiffness.

A comprehensive analysis of Figs. 6 and 7 reveals that a large main bearing stiffness improves the dynamic performance of the planet carrier but degrades the behaviors of the main bearing.

4 Conclusions

In this paper, a rigid-flexible coupled dynamic model was developed based on the analysis of the transmission principle and structural characteristics of a 2 MW wind turbine drive train. This model considered the three-point elastic support, the flexibilities of the planet carrier, and the gearbox housing. The effects of the main shaft bearing stiffness and elastic support stiffness of the torque arms on the dynamic performances of the drive train were investigated. The conclusions are presented below.

1) Variations in the elastic support stiffness of the torque

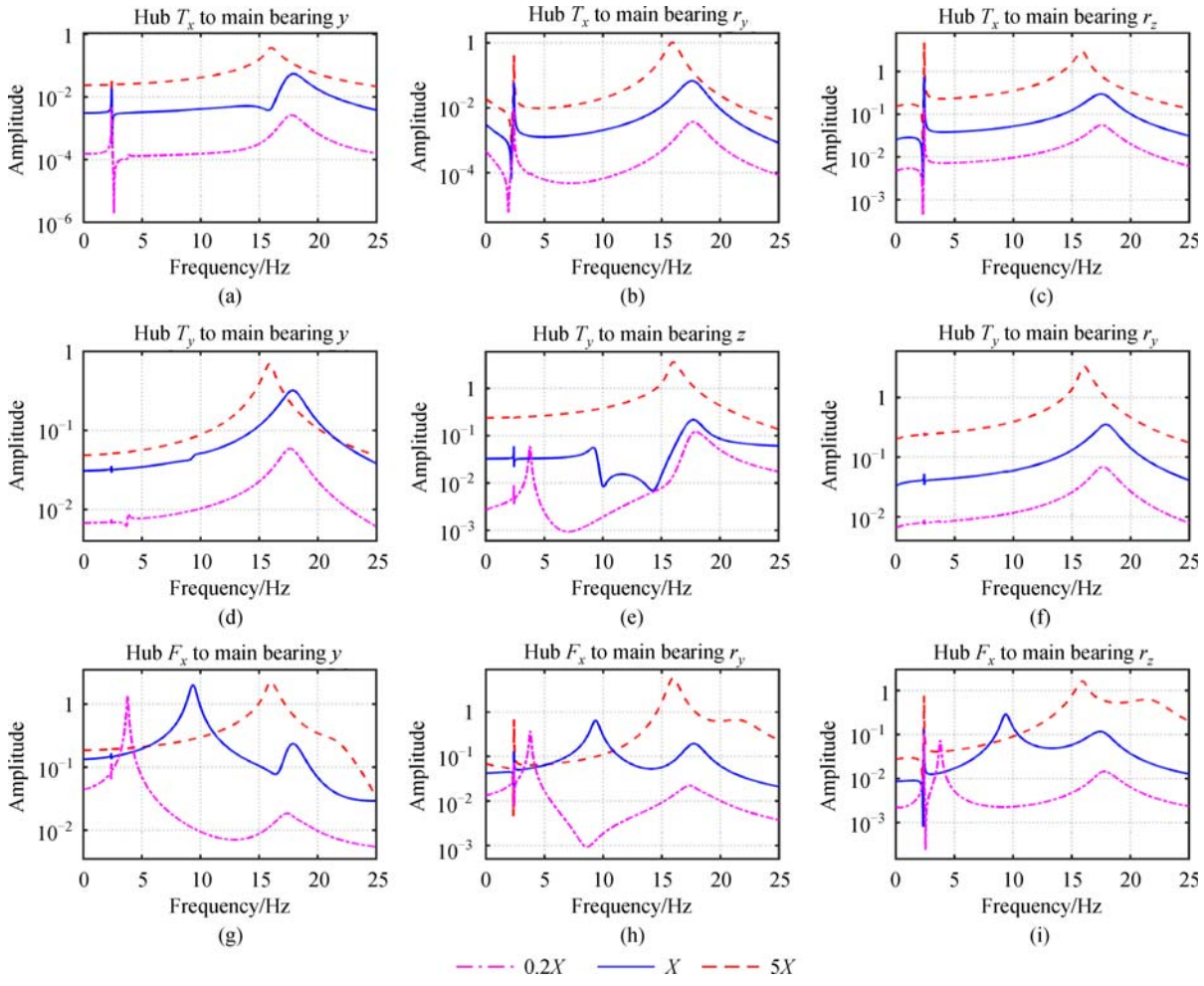

Fig. 7 FRFs between hub center excitation and main bearing response with different main bearing stiffness. (a) Hub T_x to main bearing y; (b) hub T_x to main bearing r_y; (c) hub T_x to main bearing r_z; (d) hub T_y to main bearing y; (e) hub T_y to main bearing z; (f) hub T_y to main bearing r_y; (g) hub F_x to main bearing y; (h) hub F_x to main bearing r_y; (i) hub F_x to main bearing r_z

Hub T_x to main bearing y–FRF between the hub center excitation in the T_x direction and the response in the y direction of bearing coordinate point on the main shaft

arms considerably influence the dynamic performance of both the planet carrier and the main shaft bearing. A higher elastic support stiffness of the torque arms corresponds to a weaker dynamic response of the planet carrier and the main shaft bearing, as well as a stronger elastic supporting damping, which hinders the reduction of vibration and noise in the gearbox.

2) Compared with the variations in the supporting stiffness of the torque arms, the variations in the main shaft bearing stiffness exert a weaker influence on the dynamic response of the planet carrier but a stronger influence on the main shaft bearing. Moreover, an increase in the main shaft bearing stiffness yields a weaker response in all directions of the planet carrier and a larger dynamic response of the main shaft bearing.

3) Variations in the main shaft bearing stiffness considerably affect the locations of the response peaks of both the planet carrier and the main shaft bearing. The frequency of the peak response is 9.4 Hz for the normal main shaft bearing stiffness; this value is reduced to 6.4 Hz for 0.2 times of the normal stiffness and then increased to 15.9 Hz for five times of the normal stiffness. Moreover, the frequency of the peak response is 9.4 Hz for the normal main shaft bearing stiffness; this value is reduced to 3.8 Hz for 0.2 times of the normal stiffness and then increased to 15.9 Hz for five of times the normal stiffness.

Acknowledgements The authors are grateful for the financial support given by the National Natural Science Foundation of China (Grant Nos. 51405043 and 51575060) and the Innovation Project of the City of Chongqing (Grant Nos. cstc2015zdcy-ztzx70010 and cstc2015zdcy-ztzx70012).

References

1. Guo Y, Keller J, Lacava W. Combined Effects of Gravity, Bending Moment, Bearing Clearance, and Input Torque on Wind Turbine

Planetary Gear Load Sharing: Preprint. Office of Scientific & Technical Information Technical Reports NREL/CP-5000-55968. 2012

2. Guo Y, Bergua R, Dam J V, et al. Improving wind turbine drivetrain designs to minimize the impacts of non-torque loads. Wind Energy (Chichester, England), 2014, 18(12): 2199–2222
3. Helsen J, Peeters P, Vanslambrouck K, et al. The dynamic behavior induced by different wind turbine gearbox suspension methods assessed by means of the flexible multibody technique. Renewable Energy, 2014, 69(3): 336–346
4. Helsen J, Vanhollebeke F, Marrant B, et al. Multibody modelling of varying complexity for modal behaviour analysis of wind turbine gearboxes. Renewable Energy, 2011, 36(11): 3098–3113
5. Jin X, Li L, Ju W, et al. Multibody modeling of varying complexity for dynamic analysis of large-scale wind turbines. Renewable Energy, 2016, 90: 336–351
6. He Y, Huang W, Li C, et al. Multi flexible body dynamics modeling and simulation analysis of large scale wind turbine drive train. Journal of Mechanical Engineering, 2014, 50(1): 61–69 (in Chinese)
7. Ericson T M, Parker R G. Experimental measurement of the effects of torque on the dynamic behavior and system parameters of planetary gears. Mechanism and Machine Theory, 2014, 74(74): 370–389
8. Zhao M, Ji J. Nonlinear torsional vibrations of a wind turbine gearbox. Applied Mathematical Modelling, 2015, 39(16): 4928–4950
9. Wei S, Zhao J, Han Q, et al. Dynamic response analysis on torsional vibrations of wind turbine geared transmission system with uncertainty. Renewable Energy, 2015, 78: 60–67
10. Yi P, Zhang C, Guo L, et al. Dynamic modeling and analysis of load sharing characteristics of wind turbine gearbox. Advances in Mechanical Engineering, 2015, 7(3): 1–16
11. Zhu C, Xu X, Liu H, et al. Research on dynamical characteristics of wind turbine gearboxes with flexible pins. Renewable Energy, 2014, 68(7): 724–732
12. Zhu C, Chen S, Liu H, et al. Dynamic analysis of the drive train of a wind turbine based upon the measured load spectrum. Journal of Mechanical Science and Technology, 2014, 28(6): 2033–2040
13. Zhai H, Zhu C, Song C, et al. Influences of carrier assembly errors on the dynamic characteristics for wind turbine gearbox. Mechanism and Machine Theory, 2016, 103: 138–147
14. ISO. International Standard ISO 6336-1 Second Edition, 2007
15. SIMPACK. Retrieved from http://www.simpack.com/
16. Link H, Lacava W, van Dam J, et al. Gearbox Reliability Collaborative Project Report: Findings from Phase 1 and Phase 2 Testing. Office of Scientific & Technical Information Technical Reports NREL/TP-5000-51885. 2011
17. Keller J, Guo Y, Lacava W, et al. Gearbox Reliability Collaborative Phase 1 and 2: Testing and Modeling Results; Preprint. Office of Scientific & Technical Information Technical Reports NREL/CP-5000-55207. 2012
18. LaCava W, van Dam J, Wallen R, et al. NREL Gearbox Reliability Collaborative: Comparing In-Field Gearbox Response to Different Dynamometer Test Conditions: Preprint. Office of Scientific & Technical Information Technical Reports NREL/CP-5000-51690. 2011
19. Helsen J. The dynamics of high power density gear units with focus on the wind turbine application. Dissertation for the Doctoral Degree. Louvain: Catholic University of Louvain, 2012
20. Keller J A, Guo Y, Sethuraman L. Gearbox Reliability Collaborative Investigation of Gearbox Motion and High-Speed-Shaft Loads. Office of Scientific & Technical Information Technical Reports NREL/TP-5000-65321. 2016
21. Huang W. Multibody system modeling and simulation analysis and research on dynamic characteristic of wind turbine. Dissertation for the Master's Degree. Chongqing: Chongqing University, 2013 (in Chinese)